

The boundary element method and its application to the Ice Cloud Imager for assimilation of cloud affected microwave radiances in NWP models

Antigoni Kleanthous, University College London, UK

Timo Betcke, University College London, UK

David Hewett, University College London, UK

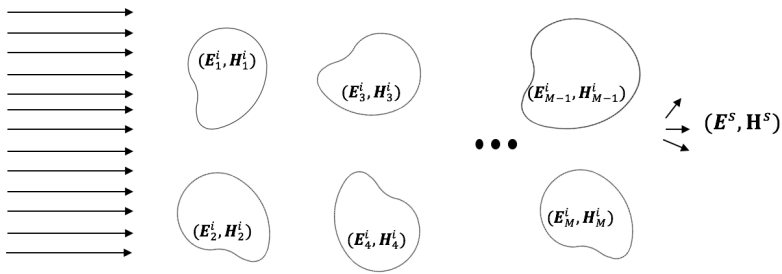
Anthony Baran, The Met Office, UK & University of Hertfordshire, UK



Plan

- The scattering problem
- The Boundary Element Method
- Preconditioning
- Bempp and Bempp-cl: Boundary Element Software
- Numerical Benchmarks
- Application to aggregates

The scattering problem



$(\mathbf{E}^{inc}, \mathbf{H}^{inc})$

- $(\mathbf{E}_m^i, \mathbf{H}_m^i)$ and $(\mathbf{E}^e, \mathbf{H}^e)$: interior and exterior fields with

$$\mathbf{E}^e = \mathbf{E}^{inc} + \mathbf{E}^s, \quad \mathbf{H}^e = \mathbf{H}^{inc} + \mathbf{H}^s,$$

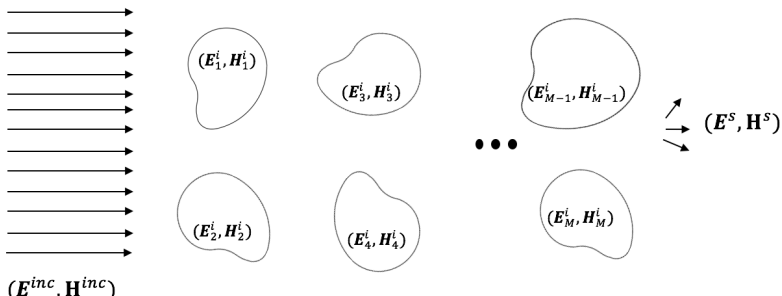
- Time-harmonic Maxwell equations

$$\begin{aligned} \nabla \times \mathbf{E}_m^i &= i\omega\mu_m \mathbf{H}_m^i, & \nabla \times \mathbf{H}_m^i &= -i\omega\epsilon_m \mathbf{E}_m^i, & \text{in } \Omega_m^i, \\ \nabla \times \mathbf{E}^e &= i\omega\mu_e \mathbf{H}^e, & \nabla \times \mathbf{H}^e &= -i\omega\epsilon_e \mathbf{E}^e & \text{in } \Omega^e, \end{aligned}$$

- Transmission boundary conditions

$$\mathbf{E}_m^i(\mathbf{x}) \times \mathbf{n} = \mathbf{E}^e(\mathbf{x}) \times \mathbf{n}, \quad \mathbf{H}_m^i(\mathbf{x}) \times \mathbf{n} = \mathbf{H}^e(\mathbf{x}) \times \mathbf{n}, \quad \mathbf{x} \in \Gamma_m.$$

The scattering problem



$(\mathbf{E}^{inc}, \mathbf{H}^{inc})$

- $(\mathbf{E}_m^i, \mathbf{H}_m^i)$ and $(\mathbf{E}^e, \mathbf{H}^e)$: interior and exterior fields with

$$\mathbf{E}^e = \mathbf{E}^{inc} + \mathbf{E}^s, \quad \mathbf{H}^e = \mathbf{H}^{inc} + \mathbf{H}^s,$$

- Time-harmonic Maxwell equations

$$\nabla \times (\nabla \times \mathbf{E}_m^i) - k_m^2 \mathbf{E}_m^i = 0, \quad \text{in } \Omega_m^i,$$
$$\nabla \times (\nabla \times \mathbf{E}^e) - k_e^2 \mathbf{E}^e = 0, \quad \text{in } \Omega^e,$$

- Transmission boundary conditions

$$\mathbf{E}_m^i(\mathbf{x}) \times \mathbf{n} = \mathbf{E}^e(\mathbf{x}) \times \mathbf{n}, \quad \mathbf{x} \in \Gamma_m$$

- reformulate the problem as boundary integral equations on the boundary Γ

- reformulate the problem as boundary integral equations on the boundary Γ
- solve the problem on the boundary

- reformulate the problem as boundary integral equations on the boundary Γ
- solve the problem on the boundary
- extend the solution to the domain of interest (e.g. interior/exterior of scatterer) via representation formulae

Why the Boundary Element Method



- lower dimensional manifold to discretise

Why the Boundary Element Method



- lower dimensional manifold to discretise
- automatically incorporates outgoing behaviour at infinity

Why the Boundary Element Method

- lower dimensional manifold to discretise
- automatically incorporates outgoing behaviour at infinity
- flexibility with geometry; it can handle complex domains such as ice crystals

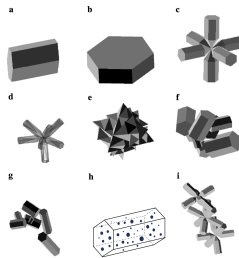


Figure: Ice Models. Taken from (Baran, 2012).

Boundary Integral Operators

- Electric and Magnetic Potential Operators

$$\mathcal{E}\mathbf{v}(\mathbf{x}) := ik \int_{\Gamma} \mathbf{v}(\mathbf{y}) G(\mathbf{x}, \mathbf{y}) d\Gamma(\mathbf{y}) - \frac{1}{ik} \nabla_{\mathbf{x}} \int_{\Gamma} \nabla_{\mathbf{y}} \cdot \mathbf{v}(\mathbf{y}) G(\mathbf{x}, \mathbf{y}) d\Gamma(\mathbf{y}),$$

$$\mathcal{H}\mathbf{v}(\mathbf{x}) := \nabla_{\mathbf{x}} \times \int_{\Gamma} \mathbf{v}(\mathbf{y}) G(\mathbf{x}, \mathbf{y}) d\Gamma(\mathbf{y}),$$

where $G(x, y) = \frac{\exp(ik|x-y|)}{4\pi|x-y|}$

- Dirichlet and Neumann Traces

$$\gamma_D^\pm \mathbf{u}(\mathbf{x}) := \mathbf{u}(\mathbf{x}) \times \mathbf{n}, \quad \gamma_N^\pm \mathbf{u}(\mathbf{x}) := \frac{1}{ik} \gamma_D^\pm (\nabla \times \mathbf{u}(\mathbf{x})), \quad \mathbf{x} \in \Gamma$$

- Boundary Integral Operators

$$\mathcal{S} := \{\gamma_D\}\mathcal{E} = -\{\gamma_N\}\mathcal{H},$$

$$\mathcal{C} := \{\gamma_D\}\mathcal{H} = \{\gamma_N\}\mathcal{E},$$

- Stratton Chu Representation Formulae

$$\mathcal{H}_m^i(\gamma_{D,m}^- \mathbf{E}_m^i) + \mathcal{E}_m^i(\gamma_{N,m}^- \mathbf{E}_m^i) = \begin{cases} \mathbf{E}_m^i(\mathbf{x}), & \mathbf{x} \in \Omega_m^i, \\ \mathbf{0}, & \mathbf{x} \notin \overline{\Omega_m^i}, \end{cases}$$

$$-\sum_m^M \mathcal{H}_m^e(\gamma_{D,m}^+ \mathbf{E}^s) - \sum_m^M \mathcal{E}_m^e(\gamma_{N,m}^+ \mathbf{E}^s) = \begin{cases} \mathbf{E}^s(\mathbf{x}), & \mathbf{x} \in \Omega_e, \\ \mathbf{0}, & \mathbf{x} \notin \overline{\Omega_e}, \end{cases}$$

The PMCHWT formulation



$$\mathcal{A}\mathbf{u}^s = \left(\frac{1}{2}\mathcal{I} - \mathcal{A}^i \right) \mathbf{u}^{inc}$$

The PMCHWT formulation

$$\mathcal{A}\mathbf{u}^s = \left(\frac{1}{2}\mathcal{I} - \mathcal{A}^i \right) \mathbf{u}^{inc}$$

$$\mathcal{A} = \begin{bmatrix} \mathcal{A}_1^e + \mathcal{A}_1^i & \mathcal{A}_{12} & \cdots & \mathcal{A}_{1M} \\ \mathcal{A}_{21} & \ddots & \ddots & \vdots \\ \vdots & \ddots & \ddots & \mathcal{A}_{(M-1)M} \\ \mathcal{A}_{M1} & \cdots & \mathcal{A}_{M(M-1)} & \mathcal{A}_M^e + \mathcal{A}_M^i \end{bmatrix}, \quad \mathcal{A}^i = \begin{bmatrix} \mathcal{A}_1^i & 0 & \cdots & 0 \\ 0 & \ddots & \ddots & \vdots \\ \vdots & \ddots & \ddots & 0 \\ 0 & \cdots & 0 & \mathcal{A}_M^i \end{bmatrix},$$

$$\mathcal{I} = \begin{bmatrix} \mathcal{I}_1 & 0 & \cdots & 0 \\ 0 & \ddots & \ddots & \vdots \\ \vdots & \ddots & \ddots & 0 \\ 0 & \cdots & 0 & \mathcal{I}_M \end{bmatrix}, \quad \mathbf{u}^s = \begin{bmatrix} \mathbf{u}_1^s \\ \mathbf{u}_2^s \\ \vdots \\ \mathbf{u}_M^s \end{bmatrix}, \quad \mathbf{u}^{inc} = \begin{bmatrix} \mathbf{u}_1^{inc} \\ \mathbf{u}_2^{inc} \\ \vdots \\ \mathbf{u}_M^{inc} \end{bmatrix}.$$

The PMCHWT formulation

$$\mathcal{A} = \begin{bmatrix} \mathcal{A}_1^e + \mathcal{A}_1^i & \mathcal{A}_{12} & & \cdots & & \mathcal{A}_{1M} \\ & \ddots & \ddots & & & \vdots \\ & & \ddots & \ddots & \ddots & \vdots \\ & & & \ddots & \ddots & \mathcal{A}_{(M-1)M} \\ \vdots & & & & \ddots & \\ \mathcal{A}_{M1} & \cdots & \mathcal{A}_{M(M-1)} & \mathcal{A}_M^e + \mathcal{A}_M^i & & \end{bmatrix}, \mathbf{u}^s = \begin{bmatrix} \mathbf{u}_1^s \\ \mathbf{u}_2^s \\ \vdots \\ \mathbf{u}_M^s \end{bmatrix},$$

where

$$\mathcal{A}_m^i = \begin{bmatrix} \mathcal{C}_m^i & \frac{\mu_m}{k_m} \mathcal{S}_m^i \\ -\frac{k_m}{\mu_m} \mathcal{S}_m^i & \mathcal{C}_m^i \end{bmatrix}, \quad \mathcal{A}_m^e = \begin{bmatrix} \mathcal{C}_m^e & \frac{\mu_e}{k_e} \mathcal{S}_m^e \\ -\frac{k_e}{\mu_e} \mathcal{S}_m^e & \mathcal{C}_m^e \end{bmatrix},$$
$$\mathcal{A}_{m\ell} = \begin{bmatrix} \mathcal{C}_{m\ell}^e & \frac{\mu_e}{k_e} \mathcal{S}_{m\ell}^e \\ -\frac{k_e}{\mu_e} \mathcal{S}_{m\ell}^e & \mathcal{C}_{m\ell}^e \end{bmatrix}, \quad \mathbf{u}_m^i = \begin{bmatrix} \gamma_{D,m}^- \mathbf{E}_m^i \\ \frac{k_m}{\mu_m} \gamma_{N,m}^- \mathbf{E}_m^i \end{bmatrix}, \quad \mathbf{u}_m^s = \begin{bmatrix} \gamma_{D,m}^+ \mathbf{E}^s \\ \frac{k_e}{\mu_e} \gamma_{N,m}^+ \mathbf{E}^s \end{bmatrix}.$$

Preconditioning: single particle case



$$\mathcal{P}\mathcal{A}\mathbf{u}^s = \mathcal{P} \left(\frac{1}{2} \mathcal{I} - \mathcal{A}^i \right) \mathbf{u}^{inc}$$

Kristof Cools, Francesco P Andriulli, and Eric Michielssen (2011). “A Calderón multiplicative preconditioner for the PMCHWT integral equation”. In: *IEEE transactions on Antennas and Propagation* 59.12, pp. 4579–4587

Preconditioning: single particle case



$$\mathcal{A}^2 \mathbf{u}^s = \mathcal{A} \left(\frac{1}{2} \mathcal{I} - \mathcal{A}^i \right) \mathbf{u}^{inc}$$

Kristof Cools, Francesco P Andriulli, and Eric Michielssen (2011). “A Calderón multiplicative preconditioner for the PMCHWT integral equation”. In: *IEEE transactions on Antennas and Propagation* 59.12, pp. 4579–4587

$$\mathcal{A}\mathbf{u}^s = \left(\frac{1}{2}\mathcal{I} - \mathcal{A}^i \right) \mathbf{u}^{inc}$$

Full Calderón preconditioning:

$$\mathcal{A}^2\mathbf{u}^s = \mathcal{A} \left(\frac{1}{2}\mathcal{I} - \mathcal{A}^i \right) \mathbf{u}^{inc}$$

$$\mathcal{A}\mathbf{u}^s = \left(\frac{1}{2}\mathcal{I} - \mathcal{A}^i \right) \mathbf{u}^{inc}$$

Full Calderón preconditioning:

$$\mathcal{A}^2\mathbf{u}^s = \mathcal{A} \left(\frac{1}{2}\mathcal{I} - \mathcal{A}^i \right) \mathbf{u}^{inc}$$

Diagonal Calderón preconditioning:

$$\mathcal{D}\mathcal{A}\mathbf{u}^s = \mathcal{D} \left(\frac{1}{2}\mathcal{I} - \mathcal{A}^i \right) \mathbf{u}^{inc}$$

Discrete Systems: Weak and Strong Forms

**UCL**

Continuous operator	Discrete Weak Form	Discrete Strong Form
\mathcal{A}	$\mathbf{A}\mathbf{x} = \mathbf{b}$	$\mathbf{M}^{-1}\mathbf{A}\mathbf{x} = \mathbf{M}^{-1}\mathbf{b}$
\mathcal{A}^2	$\mathbf{A}\mathbf{M}^{-1}\mathbf{A}\mathbf{x} = \mathbf{A}\mathbf{M}^{-1}\mathbf{b}$	$\mathbf{M}^{-1}\mathbf{A}\mathbf{M}^{-1}\mathbf{A}\mathbf{x} = \mathbf{M}^{-1}\mathbf{A}\mathbf{M}^{-1}\mathbf{b}$
$\mathcal{D}\mathcal{A}$	$\mathbf{D}\mathbf{M}^{-1}\mathbf{A}\mathbf{x} = \mathbf{D}\mathbf{M}^{-1}\mathbf{b}$	$\mathbf{M}^{-1}\mathbf{D}\mathbf{M}^{-1}\mathbf{A}\mathbf{x} = \mathbf{M}^{-1}\mathbf{D}\mathbf{M}^{-1}\mathbf{b}$

- matvec: a single application of one discretised boundary integral operator \mathcal{C}_m^i , \mathcal{C}_m^e , \mathcal{S}_m^i , \mathcal{S}_m^e . Applications of \mathbf{M}^{-1} not taken into account

Total cost of operators:

$$\mathcal{A} : 4M(M + 1)(G + \lfloor G/\rho \rfloor) \text{ matvecs}$$

$$\mathcal{A}^2 : 8M(M + 1)(G + \lfloor G/\rho \rfloor) + 4M(M + 1) \text{ matvecs}$$

$$\mathcal{D}\mathcal{A} : 4M(M + 3)(G + \lfloor G/\rho \rfloor) + 8M \text{ matvecs}$$

G : number of GMRES iterations

ρ : number of iterations per GMRES cycle

Bempp: Boundary Element Software



bempp
services

HOME

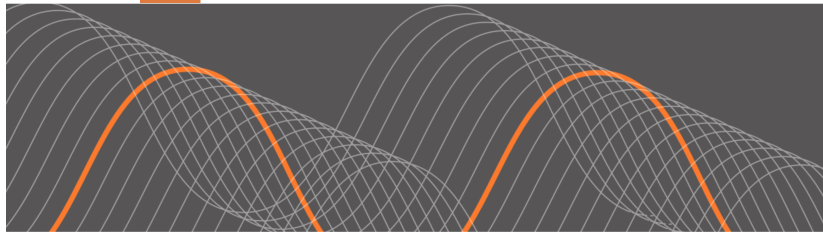
DOCUMENTATION

PUBLICATIONS

SUPPORT

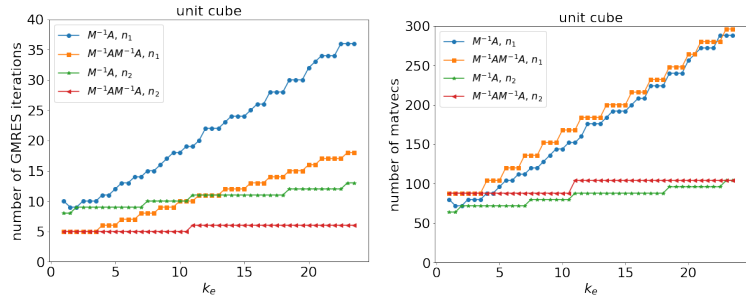
TEAM

COMMERCIAL



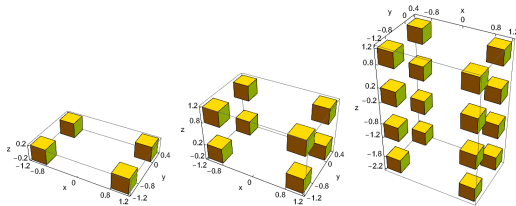
- open source: www.bempp.com
- new GPU version available soon

Benchmarks: single particle scattering



$$n_1 = 1.311 + 2.289 \times 10^{-9}i, \quad n_2 = 1.0833 + 0.204i$$

Antigoni Kleanthous et al. (2019). “Calderón preconditioning of PMCHWT boundary integral equations for scattering by multiple absorbing dielectric particles”. In: *Journal of Quantitative Spectroscopy and Radiative Transfer* 224, pp. 383–395



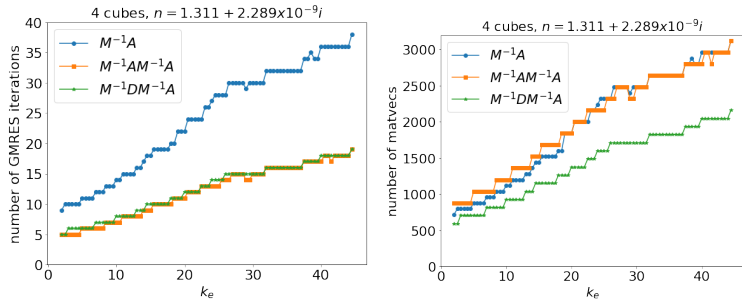
$$n = 1.311 + 2.289 \times 10^{-9} i$$

	4 cubes	8 cubes	16 cubes
Discrete operator			
$\mathbf{M}^{-1}\mathbf{A}$	22 (1840)	24 (7200)	32 (35904)
$\mathbf{M}^{-1}\mathbf{A}\mathbf{M}^{-1}\mathbf{A}$	11 (1840)	12 (7200)	16 (35904)
$\mathbf{M}^{-1}\mathbf{D}\mathbf{M}^{-1}\mathbf{A}$	12 (1376)	12 (4288)	16 (19584)

Antigoni Kleanthous et al. (2019). “Calderón preconditioning of PMCHWT boundary integral equations for scattering by multiple absorbing dielectric particles”. In: *Journal of Quantitative Spectroscopy and Radiative Transfer* 224, pp. 383–395.



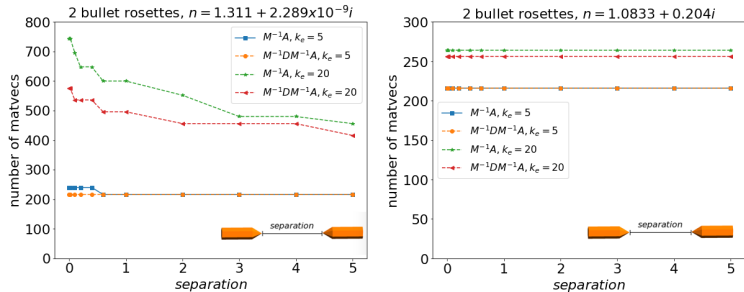
Benchmarks: multi-particle scattering ($M = 4$)



Antigoni Kleanthous et al. (2019). “Calderón preconditioning of PMCHWT boundary integral equations for scattering by multiple absorbing dielectric particles”. In: *Journal of Quantitative Spectroscopy and Radiative Transfer* 224, pp. 383–395.

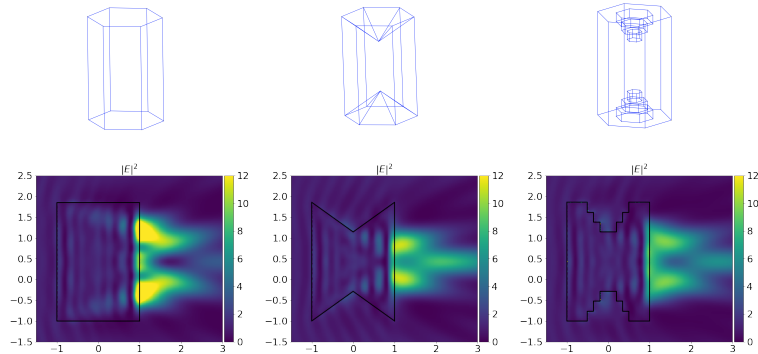


Benchmarks: distance of scatterers



Antigoni Kleanthous et al. (2019). "Calderón preconditioning of PMCHWT boundary integral equations for scattering by multiple absorbing dielectric particles". In: *Journal of Quantitative Spectroscopy and Radiative Transfer* 224, pp. 383–395

Numerical Examples: single scattering



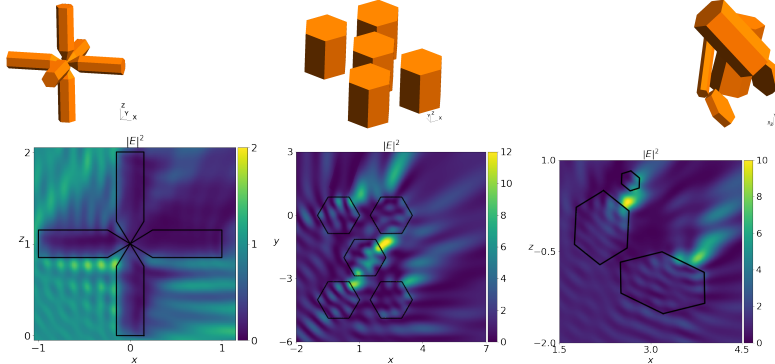
$$n = 1.311 + 2.289 \times 10^{-9} i$$

Discrete operator

$$\begin{array}{lll} \mathbf{M}^{-1}\mathbf{A} & 34 \text{ (280)} & 30 \text{ (248)} \\ \mathbf{M}^{-1}\mathbf{A}\mathbf{M}^{-1}\mathbf{A} & 17 \text{ (280)} & 15 \text{ (248)} \end{array}$$

Antigoni Kleanthous et al. (2019). “Calderón preconditioning of PMCHWT boundary integral equations for scattering by multiple absorbing dielectric particles”. In: *Journal of Quantitative Spectroscopy and Radiative Transfer* 224, pp. 383–395

Numerical Examples: multiple scattering

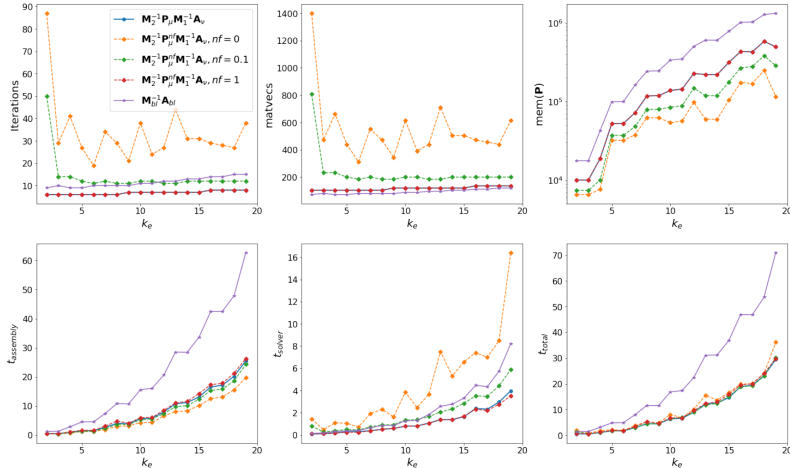


Discrete operator

$\mathbf{M}^{-1}\mathbf{A}$	15 (2520)	52 (6480)	142 (17880)
$\mathbf{M}^{-1}\mathbf{A}\mathbf{M}^{-1}\mathbf{A}$	8 (2856)	25 (6360)	63 (15960)
$\mathbf{M}^{-1}\mathbf{D}\mathbf{M}^{-1}\mathbf{A}$	8 (1776)	23 (3880)	61 (10280)

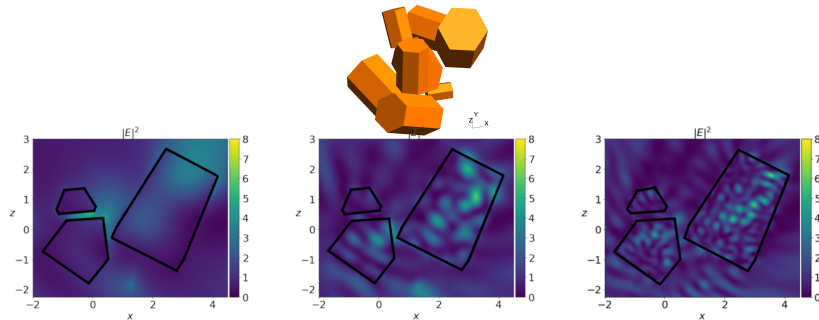
Antigoni Kleanthous et al. (2019). “Calderón preconditioning of PMCHWT boundary integral equations for scattering by multiple absorbing dielectric particles”. In: *Journal of Quantitative Spectroscopy and Radiative Transfer* 224, pp. 383–395

Accelerated Preconditioning: Benchmarks



Kleanthous Antigoni et al. "Accelerated Calderón preconditioning for Maxwell problems". In: Preparation ()

Numerical Benchmarks: ice crystals



f	refractive index n	dofs	$\mathbf{M}_{bl}^{-1}\mathbf{P}_{bl}\mathbf{M}_{bl}^{-1}\mathbf{A}_{bl}$			$\mathbf{M}_2^{-1}\mathbf{P}_{\mu}^{nf}\mathbf{M}_1^{-1}\mathbf{A}_{\nu}$		
			Iters	$t_{assembly}$	t_{solver}	t_{total}	Iters	$t_{assembly}$
50	$1.7754 + 0.00066i$	2556	46	1.9	1.0	2.9	113	0.26
183	$1.7754 + 0.00243i$	26421	303	25.2	76.9	102.1	429	3.8
325	$1.7754 + 0.0044i$	81318	-	-	-	-	300	11.5
								57.3
								68.8

Kleanthous Antigoni et al. "Accelerated Calderón preconditioning for Maxwell problems". In: Preparation ()

- Mid September - Mid December
- working with Anthony Baran
- goal is to simulate single scattering properties and phase matrices of aggregates of bullet rosettes in random orientation
- 5 temperatures: 190.0K, 210.0K, 230.0K, 250.0K, 270.0K
- 4 frequencies: 50GHz, 183GHz, 243GHz, 664GHz
- range of sizes ranging from μm to cm .

Aggregate Model

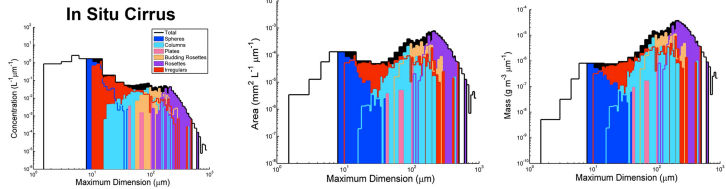
Table A1
Projects

Acronym	Acronym expanded	Primary sponsor(s)
ACTIVE	Aerosol and Chemical Transport in Tropical Convection	UK NERC
ATREX	Airborne Tropical Tropopause Experiment	NASA
CCCOPE	Cooperative Convective Precipitation Experiment	NSF/BOR
CR-AVE	Costa Rica AURA Validation Experiment	NASA
CRYSTAL-FACE	Cirrus Regional Study of Tropical Anvils and Cirrus Layers-Florida Area Cumulus Experiment	NASA
DC3	Deep Convective Clouds and Chemistry Project	NASA/NSF
EOS	Earth Observing System	DOE
EMERALD-I & II	Egrett Microphysics Experiment with Radiation, Lidar, and Dynamics	UK NERC
FIRE.ACE	First ISCCP Regional Experiment Arctic Cloud Experiment	NASA/DOE
FIRE-II	First ISCCP Regional Experiment	NASA
ICE-T	Ice in Clouds Experiment-Tropical	NSF
ISDAC	Indirect and Semi-Direct Aerosol Campaign	DOE, NASA
MIDCIX	Midlatitude Cirrus Cloud Experiment	DOE
POSIDON	Pacific Oxidants, Sulfur, Ice, Dehydration, and Convection Experiment	NASA
SEAC4RS	Studies of Emissions and Atmospheric Composition, Clouds and Climate Coupling by Regional Surveys	NASA
SCCP	Sierra Cooperative Pilot Project	BOR
SPARTICUS	Small Particles in Cirrus Project	DOE
TC4	Tropical Composition, Cloud and Climate Coupling	NASA
TRMM KWAJEX	Tropical Rain Measurement Mission Kwajalein Experiment	NASA
TRMM TEFLUN-A	TRMM Texas and Florida Under Flights – A (Texas)	NASA
TRMM TEFLUN-B	TRMM Texas and Florida Under Flights – B (Florida)	NASA
TWP-ICE	Tropical Warm Pool – International Cloud Experiment	DOE

- The study grouped together more than 107 CPI images.
- Goal: to see if the ice crystal shape distributions differ from varying ice cloud regimes.
- Which shape distribution should we initially use for the microwave and sub-mm (i.e. sizes 100 – 10000 μm) ?

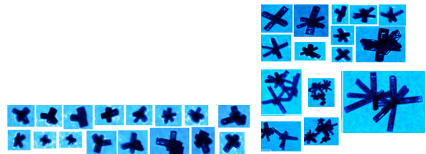
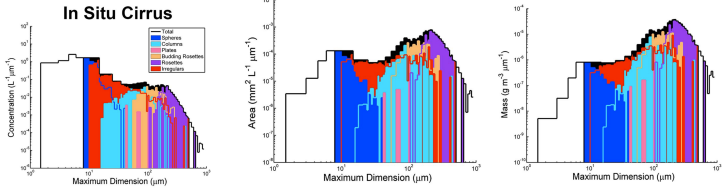
RP Lawson et al. (2019). "A Review of Ice Particle Shapes in Cirrus formed In Situ and in Anvils". In: *Journal of Geophysical Research: Atmospheres* 124.17-18, pp. 10049–10090

Aggregate Model



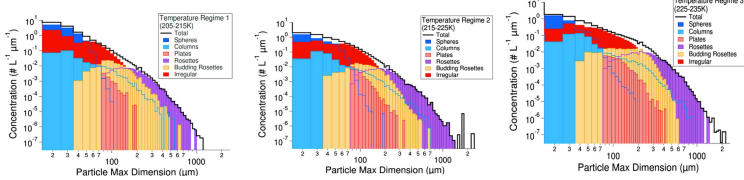
RP Lawson et al. (2019). "A Review of Ice Particle Shapes in Cirrus formed In Situ and in Anvils". In: *Journal of Geophysical Research: Atmospheres* 124.17-18, pp. 10049–10090

Aggregate Model



RP Lawson et al. (2019). "A Review of Ice Particle Shapes in Cirrus formed In Situ and in Anvils". In: *Journal of Geophysical Research: Atmospheres* 124.17-18, pp. 10049–10090

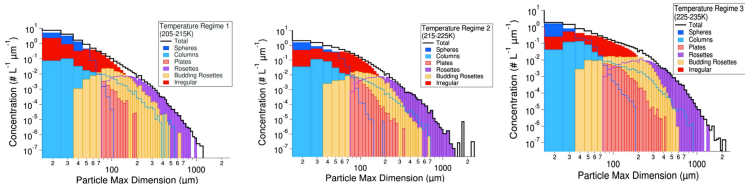
Aggregate Model



RP Lawson et al. (2019). "A Review of Ice Particle Shapes in Cirrus formed In Situ and in Anvils". In: *Journal of Geophysical Research: Atmospheres* 124.17-18, pp. 10049–10090

RJ Cotton et al. (2013). "The effective density of small ice particles obtained from in situ aircraft observations of mid-latitude cirrus". In: *Quarterly Journal of the Royal Meteorological Society* 139.676, pp. 1923–1934

Aggregate Model



For an initial shape distribution to represent scattering in *mm*-wave and sub-*mm*-wave, the rosettes and aggregates of these seem reasonable to assume. Construct rosette mass models such that:

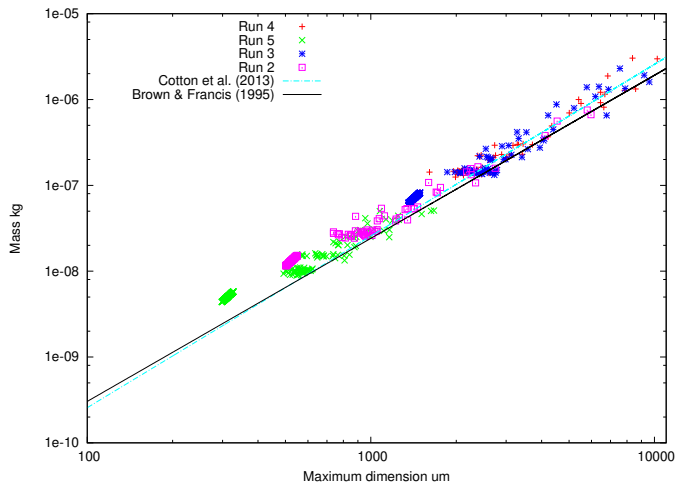
- mass $\approx D^3$, for budding rosettes
- mass = $0.0257D^2$, for rosette aggregates, following Cotton et al. (2013) within $\pm 30\%$

RP Lawson et al. (2019). "A Review of Ice Particle Shapes in Cirrus formed In Situ and in Anvils". In: *Journal of Geophysical Research: Atmospheres* 124.17-18, pp. 10049–10090

RJ Cotton et al. (2013). "The effective density of small ice particles obtained from in situ aircraft observations of mid-latitude cirrus". In: *Quarterly Journal of the Royal Meteorological Society* 139.676, pp. 1923–1934

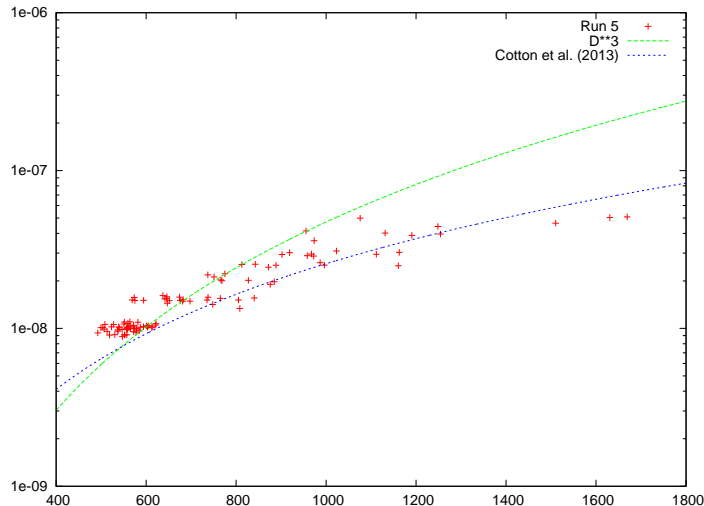
Aggregate Model

In collaboration with Chris Westbrook, University of Reading.



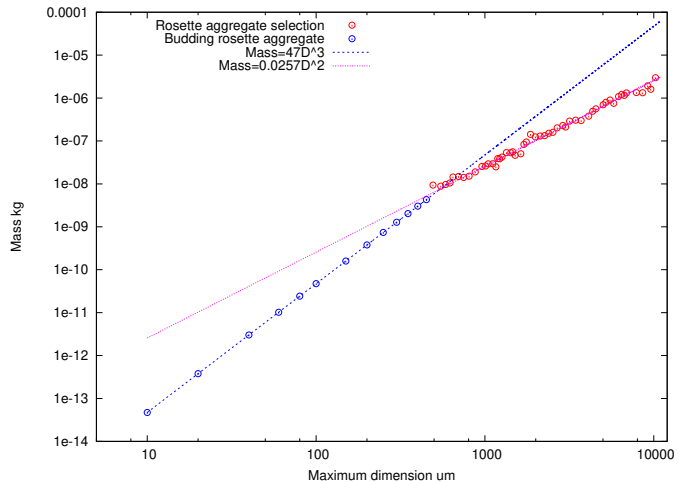
Aggregate Model

In collaboration with Chris Westbrook, University of Reading.

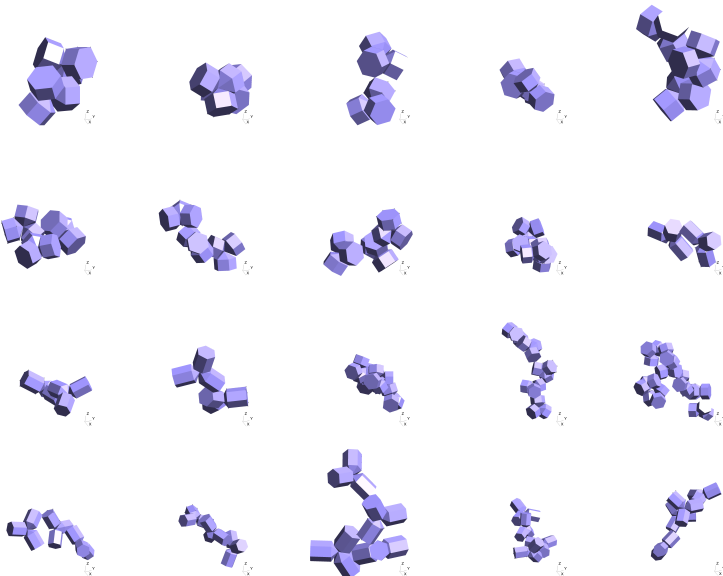


Aggregate Model

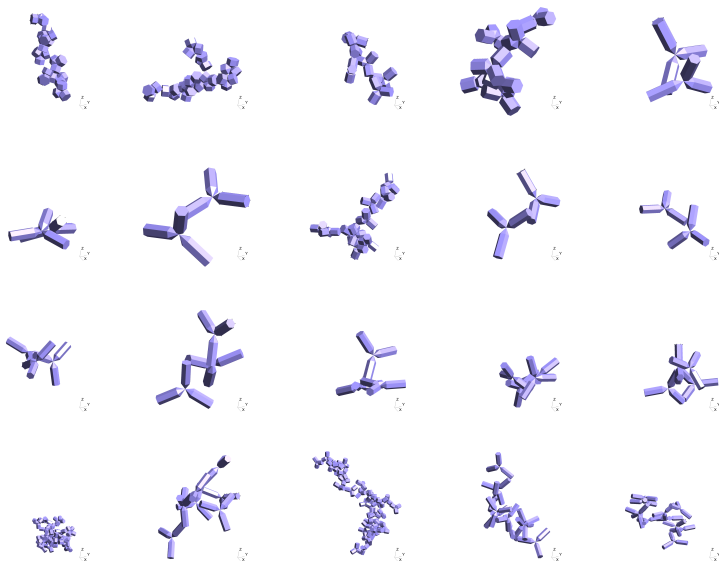
In collaboration with Chris Westbrook, University of Reading.



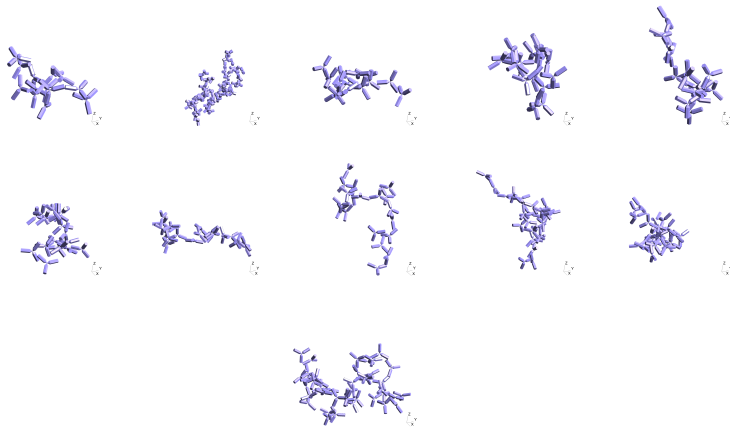
Aggregate Model



Aggregate Model



Aggregate Model



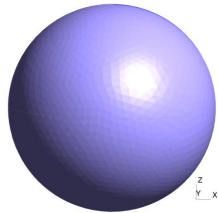
- Usually the orientational average of a quantity Q is calculated by

$$\langle Q \rangle = \frac{1}{8\pi^2} \int_0^{2\pi} d\beta \int_{-1}^1 d\cos\theta \int_0^{2\pi} d\phi Q(\beta, \theta, \phi)$$

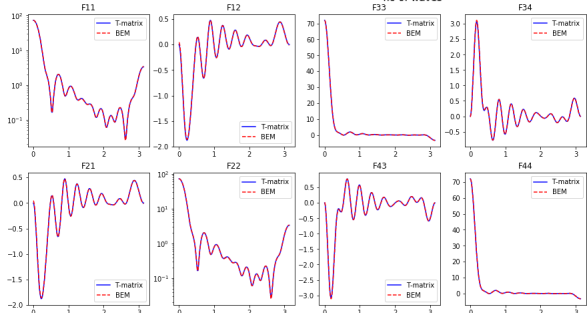
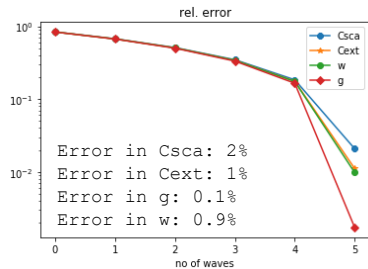
where β, θ, ϕ are the three angles that describe the orientation of the particle.

- In terms of BEM, that would require a new matrix \mathbf{A} in the system $\mathbf{Ax} = \mathbf{b}$, for each orientation.
- Instead, we fix the orientation and consider different incident waves. That way \mathbf{A} remains the same, only \mathbf{b} changes saving computational time and memory.

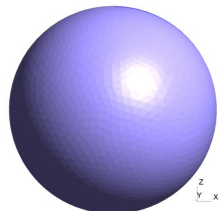
Testing: sphere X=10



Radius = 719 μm
Refractive index = $1.7746 + 0.00940j$
Frequency = 664GHz
Mesh: 10 elements per wavelength
Elements: 7808



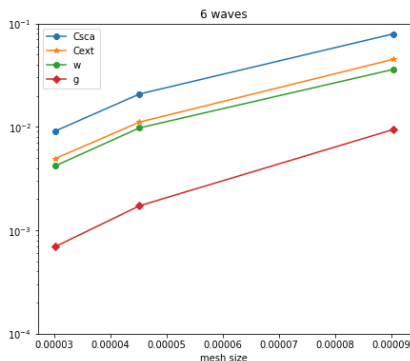
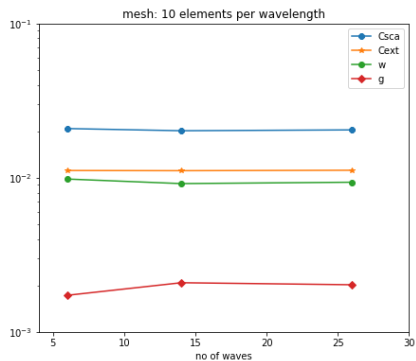
Testing: sphere X=10



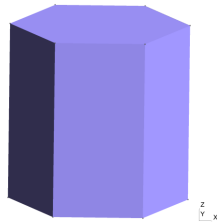
Radius = 719 μm

Refractive index = $1.7746 + 0.00940j$

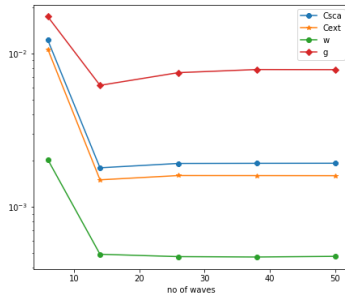
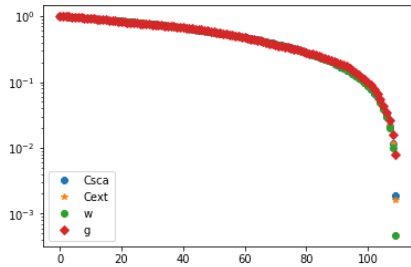
Frequency = 664GHz



Testing: hexagonal column X=1



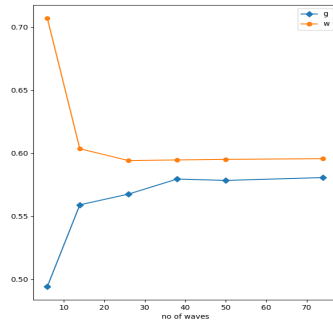
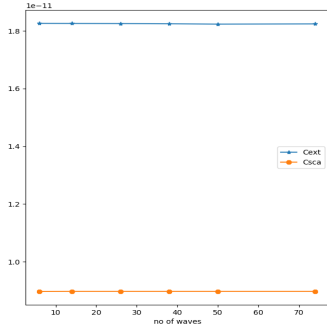
Refractive index = $1.7746+0.00064j$
Frequency = 50GHz
Mesh: 10 elements per wavelength
Elements: 180



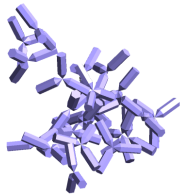
Testing: Aggregate Dmax = 492 μ m



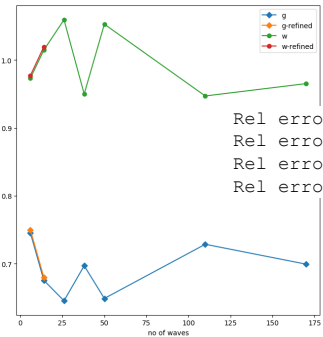
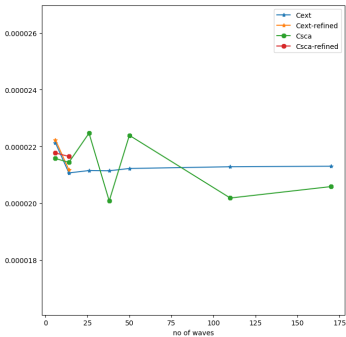
Refractive index = 1.7643+0.00042j
Frequency = 50GHz
Elements: 204



Testing: Aggregate X=70, Dmax = 9594 μm

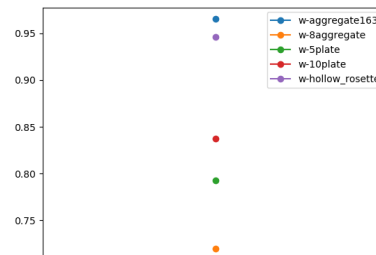
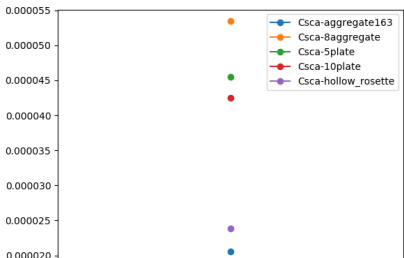
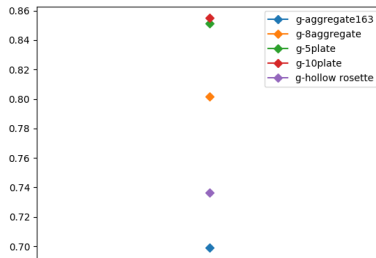
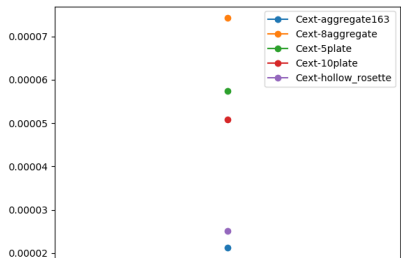


Refractive index = $1.7746+0.00064j$
Frequency = 664GHz
Elements: 51268 (usual mesh)
104866 (refined mesh)

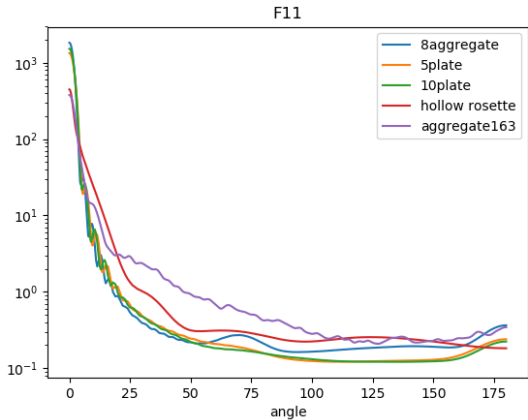


Rel error(h) in Csca: 0.9%
Rel error(h) in Cext: 0.5%
Rel error(h) in g: 0.6%
Rel error(h) in w: 0.5%

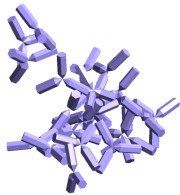
Testing: Aggregate X=70



Testing: Aggregate X=70



Testing: Aggregate X=140, Dmax = 2 cm UCL



Refractive index = 1.7746+0.00064j

Frequency = 664GHz

Elements: 190 820

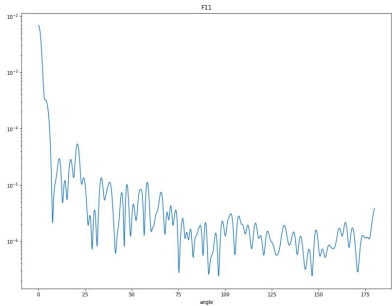
Memory ~ 200 G

Assembly time: 167 mins

Solve time for 1 wave: 126 mins

GMRES iterations: 210





- Deploy the code on AWS (64 particle sizes, 5 temperatures, 4 frequencies)
- database to be ready by March 2020
- Currently formulations hold for homogeneous particles, next step to model aerosol particles and inhomogeneous particles with inclusions.